Subsurface flaw detection in reflective materials by thermal-transfer imaging

Maldague, Xavier P.; Krapez, Jean-Claude; Cielo, Paolo G.

Publisher's version / Version de l'éditeur:
https://doi.org/10.1117/12.55760
Optical Engineering, 30, 1, pp. 117-125, 1991-01-01

Subsurface flaw detection in reflective materials by thermal transfer imaging

X. Maldague
Université Laval
Electrical Engineering Department
Québec City, Québec G1K 7P4, Canada

J.-C. Krapez
P. Cielo
National Research Council Canada
Industrial Materials Institute
75 de Mortagne Boulevard
Boucherville, Québec J4B 6Y4, Canada

Abstract. A thermal imaging apparatus is described for the nondestructive detection of subsurface defects in materials that would not usually lend themselves to thermal imaging because of their low emissivity and high susceptibility to background reflection noise. This is accomplished by transferring the thermal image produced by surface temperature perturbation of the workpiece material to a high emissivity material with which it is continuously brought in contact. The transferred thermal image may be observed by a suitable infrared device, resulting in a high radiance image with minimum reflectivity or variable emissivity noise. Numerical simulations, as well as experimental results, are presented.

Subject terms: infrared thermography; surface emissivity; transfer imaging; flaw detection; nondestructive inspection.

Optical Engineering 30(1), 117-125 (January 1991).

CONTENTS

1. INTRODUCTION

Hidden subsurface defects, such as an inclusion, a delamination, or a lack of bonding in a laminated structure, must be detected during or after manufacturing to avoid risks of in-service failure. Thermography[1–5] is an attractive technique for such nondestructive testing (NDT) of laminar materials. The standard approach for subsurface defect detection relies on the detection of temperature discontinuities on the inspected surface above the defects after heat injection over a wide area through the workpiece. In the case of a reflective approach, both the detection pickup and the thermal perturbation source are located on the same side of the workpiece. The surface temperature of the part to inspect falls rapidly after the initial heat input as heat diffuses into the material. The presence of a defect reduces the diffusion rate so that its position is revealed by a higher surface temperature above its location after the thermal front has reached the defect interface. In a transmissive configuration, heat is injected on the workpiece side opposite the surface to be inspected, and again internal defects will locally perturb heat propagation through the workpiece thickness, introducing temperature nonuniformities on the inspected side.

Heat may be injected into the workpiece by means of radiators, infrared lamps, flash lamps, or hot air guns. Alternatively, the previously heated or naturally hot material may be surface cooled by a cool-air or water jet (e.g., see Ref. 5, Fig. 10), in which case a thermal discontinuity over the defect will develop when the cold thermal front reaches the subsurface flaw. In a modern thermal imaging system, an infrared camera is used to continuously display the surface temperature of the thermally excited workpiece for inspecting relatively wide areas at a fast pace. The resulting images showing the workpiece surface temperature history may be observed readily or recorded for later (computer) analysis and archival purposes.

Infrared inspection systems are difficult to apply to the nondestructive testing of materials having reflective surfaces, such as metallic sheets or aluminum-to-aluminum adhesively bonded panels of the kind used in the transportation and aeronautical industries. Metallic surfaces have a low IR absorptivity and thus a low emissivity coefficient, typically 5% of the emissivity of a blackbody. The IR power radiated by the heated metallic workpiece is exceedingly low, giving a faint thermal image. Even worse, the presence of grease patches or slightly oxidized areas on the metal surface may easily change the local surface emissivity from 5% to 10% or 20% of the blackbody emissivity, creating apparent "hot spots" on the IR image that may be interpreted as defective areas. Moreover, the high reflectivity of the metallic surfaces introduces a reflection noise problem, whereby infrared radiation emitted by warm bodies in the background is reflected by the metal surface, which acts as a smooth mirror in the long-wavelength IR region. The reflected image superposes to the IR emission image, introducing further spurious "hot spots" and thus further complicating the interpretation of the thermal image provided by the IR camera.

One possible approach to overcome these problems requires painting the metallic surface black prior to inspection. The black painted surface has a uniformly high emissivity independent of the presence of grease patches, while its reflectivity and thus the interference problems from nearby warm bodies is exceed-

Paper 2768 received July 17, 1989; revised manuscript received June 16, 1990; accepted for publication June 30, 1990. This paper is a revision of paper 1094–27, presented at the SPIE conference Thermosense XI, March 29–31, 1989, Orlando, Florida. The paper presented there appears (unrefereed) in SPIE Proceedings Vol. 1094.

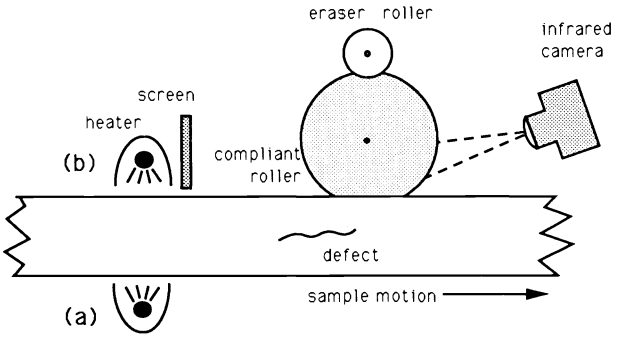

Fig. 1. Thermal transfer imaging system using a compliant roller and (a) a transmissive or (b) a reflective configuration for the detection of defects of known depth in a laminar workpiece.

ingly low. However, the introduction of a painting procedure and of a cleaning step after inspection is quite inconvenient for a technique whose main advantage, when compared to competitive nondestructive testing methods, is the high inspection speed.

Another method for reducing low emissivity problems is the use of a reflective cavity.[6] By introducing a reflective structure, such as a hemisphere, above the surface whose temperature is to be monitored, the effective emissivity is increased by multiple reflections within the cavity to near-blackbody values. Although appropriate for the average temperature sensing of a given area, this approach is inadequate for thermal imaging because multiple reflections within the cavity tend to average out the IR radiation emitted by the whole surface enclosed by the cavity. The spatial resolution required to delimit the defects would thus be lost by using such an approach.

Another possible approach to deal with the emissivity problem makes use of a surface heat transfer step.[7] The inspected surface is quickly put in contact with an intermediary medium such as a high emissivity blanket, to which the surface temperature distribution is transferred. The high emissivity medium can subsequently be inspected without the low emissivity problems mentioned above. However, good thermal image transfer and postcontact retention requirements during the inspection period place conflicting demands on the transfer medium properties.

In this paper we describe a thermal transfer technique that is particularly well adapted to a continuous NDT inspection. A compliant roller provides a transfer medium that is well suited to on-line applications. Materials having pressure-dependent thermal propagation properties are investigated in order to efficiently transfer the thermal image on contact and to reduce image fading after contact. Different experimental configurations are described and the results are discussed with reference to a thermal propagation model.

2. QUALITATIVE DESCRIPTION OF THE METHOD

The present device is adapted to the high-rate inspection of large metallic sheets or otherwise highly reflective materials. The main objective is to obtain high spatial resolution without needing any previous sample preparation or postcleaning steps. This is accomplished by introducing a back or front surface thermal perturbation on the structure to be inspected, transferring the resulting thermal image to a high emissivity material continuously brought in contact with the inspected workpiece, and imaging the temperature distribution on the high emissivity material by an infrared camera.

2.1. Fixed thermal propagation time configuration

Figure 1 shows a schematic diagram of a first configuration. The continuous sheets that must be inspected, typically an assembly of layers adhesively bonded between the top and bottom metallic surfaces, may contain hidden flaws in the form of delaminations between adjacent layers. The sheet is driven through the continuous nondestructive inspection station, including a series of rollers as well as a heating lamp, extending across the sheet in a direction perpendicular to the plane of Fig. 1.

In a transmissive configuration [Fig. 1(a)], as the lower surface of the sheet is heated when passing over the heat source, heat flows from the lower surface to the upper surface. If this heat flow encounters along its path low thermal conductivity defects, the heat flow lines will deviate to circumvent the defects, leaving a relatively cooler area on the regions of the upper surface above the defects. In a conventional IR nondestructive system, an IR camera is used to display the temperature distribution across the upper surface of the sheet, and the observation of "cold spots" is related to the presence of defects immediately below the cooler region. Alternatively [Fig. 1(b)], in a reflective configuration both the IR camera and the heat source may be located on the upper surface of the sheet; defects will manifest themselves in this case by relatively warmer areas ("hot spots") over the low thermal conductivity defects, as mentioned in the introduction. The reflective configuration is generally preferable when defects close to the upper surface are to be detected in a thick sheet, or in general when the lower surface is not easily accessible.

The difficulty in detecting hidden defects in metallic structures using the approach described is apparent if one considers that the temperature differentials that develop between defect-related hot or cold spots as compared to defect-free areas are usually in the range of a fraction of 1°C. Although modern IR cameras have sensitivities of the order of 0.1°C when pointing toward high emissivity surfaces such as black painted materials, their sensitivity degrades substantially when a low emissivity bare metal surface is inspected. Moreover, apparent temperature fluctuations by several degrees may be introduced when the IR radiation from the surrounding background is reflected by the metallic surface toward the camera.

Such problems are reduced by inserting along the inspection line a high emissivity soft roller that is freely rotating so as to be in continuous good thermal contact with the upper surface of the sheet to be thermally inspected. Heat flows from this surface to the compliant cylinder so that after the contact the temperature distribution over the surface of the compliant cylinder reproduces the temperature distribution over the surface of the metallic sheet. This temperature distribution can be conveniently observed by pointing the IR camera toward the surface of the compliant roller either directly or through a reflection from the highly reflective metallic surface (whose reflectivity is assumed to be close to unity and thus relatively constant). Because of the high IR emissivity of the compliant roller, preferably made of a black rubber or foam material, the displayed thermal image observed on the black roller has a high intensity and is unaffected by background reflections because of the low reflectivity of the black roller surface.

More precisely, the compliant roller may be made of a carbon-powder-filled foam polymer, whose internal porosity ensures a good compliance and a relatively small thermal conductivity. In the region of the roller in contact with the sheet surface, the gas bubbles inside the foam material are mainly collapsed by the

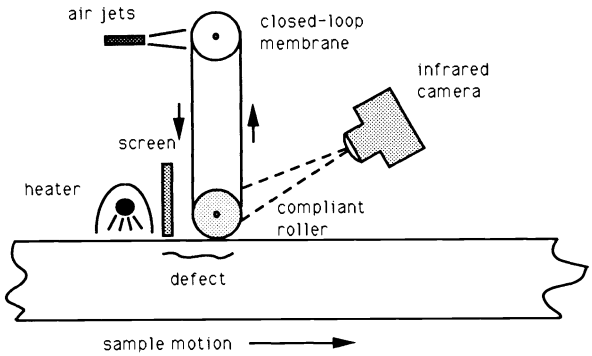

Fig. 2. Thermal transfer imaging using the same basic principles as the configuration of Fig. 1, shown in the reflective approach, with a closed-loop membrane for reduced head encumbrance and a more convenient erasure of the transferred images.

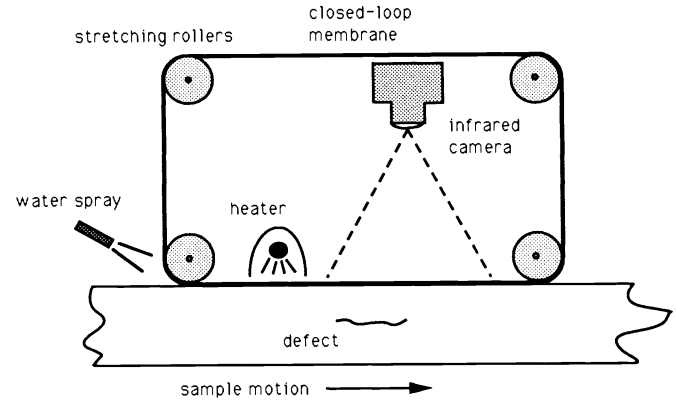

Fig. 3. Thermal transfer imaging system using a closed-loop membrane applied on the workpiece surface for the detection of defects of unknown depth.

action of the applied pressure. This results in a good thermal flow from the sheet within the cylinder during the relatively short contact time period. After contact, the air bubbles in the foam are reestablished at their original size, thus reducing thermal flow inside the roller material. As a consequence, the transferred thermal image will remain for a relatively long time and with good contrast on the surface of the roller, where it can be observed at ease by the IR camera.

An auxiliary roller, preferably made of a highly conductive metal such as copper and cooled through water circulation, is brought into contact with the compliant roller to effectively erase the thermal image on the surface. This auxiliary roller could be replaced with an air-jet curtain, but the use of a contact roller is preferred because it ensures a better temperature uniformity along the compliant roller.

It should be noticed that in the configuration shown in Fig. 1, the imaged temperature distribution corresponds to a fixed thermal propagation time, corresponding to the ratio of the heater-to-roller distance and the sheet speed. After transfer to the roller, such a distribution is "frozen" during the imaging step. Consequently, the distance between the thermal source and the roller must be appropriately chosen in relation to the sheet geometry, the line speed, and the thermal diffusivity of the sheet material. In the transmission configuration, Fig. 1(a), the time delay between heating and contact with the roller for a given sheet section must be close to the thermal propagation time $t \sim d^2/a$ through the sheet, where d is the sheet thickness and a is its thermal diffusivity. The reflection configuration, Fig. 1(b), is most effective when the above-mentioned time delay corresponds to the thermal propagation time z^2/a to the depth z of the expected defects below the heated surface. This implies that the depth of the defects is already known, as in the case where delaminations are to be detected below a layer of known thickness such as a coating or a bonded metal skin. A more general configuration is discussed in the next section.

A further point to be mentioned concerns heating uniformity. If the low-emissivity workpiece surface presents emissivity variations across its surface, it will correspondingly absorb the heat lamp energy with different absorptivities, inducing false hot spots. Such a problem can be avoided by backing the heating lamp with a parabolic reflector, as shown in Fig. 1. This results in multiple reflections between the sheet surface and the reflector, which increase the effective absorptivity to near-blackbody values independently of the actual surface absorptivity, as discussed above.

Figure 2 presents a possible variation of the basic configuration of Fig. 1. In this case a closed-loop membrane connects the compliant and auxiliary rollers together, thus reducing the space required by the thermal transfer imaging head on the workpiece surface. Another possible benefit of this modification is the ease with which the thermal image can be erased on the membrane because of its length.

2.2. Variable propagation time configuration

The systems shown in Figs. 1 or 2 are mainly useful for the inspection, in a transmission configuration, of relatively thin, sheet-like materials or else for the detection, in a reflection configuration, of shallow defects within a known depth range in a massive workpiece. When a predetermined defect depth range cannot be fixed, a different configuration may be used, as illustrated in Fig. 3. In this case, a closed-loop membrane, preferably a thin black plastic sheet, is kept in close contact with the surface of the sheet to be inspected by a system of stretching rollers. A modest-flow water jet is used to produce by capillarity a thin liquid film between the pellicle and the workpiece to ensure a good thermal contact at the interface. After surface perturbation by the thermal source, heat flows within the workpiece and is eventually distorted by the presence of subsurface defects leaving hot spots (or cold spots, for cool thermal perturbation) on the membrane surface, which are observed by an IR camera.

In contrast to the configurations shown in Figs. 1 and 2, the thermal distribution seen by the camera in Fig. 3 evolves as the surface advances. Consequently, the camera, which is necessarily a 2-D camera here, as opposed to Figs. 1 and 2 where a simple line-scanning device can be used, can detect defects of progressively larger depth as a given portion of the material moves across the camera field of view. The depth range of the defects is thus larger in the case of Fig. 3, while the actual depth of a given defect can be estimated from its maximum visibility position across the camera image. Furthermore, the eventual presence of air bubbles or other thermal discontinuities at the interface between the membrane and the workpiece may be differentiated from internal defects by observing that the visibility of interface defects does not increase during the advancement of the workpiece.

3. THEORETICAL ASPECTS OF THE THERMAL TRANSFER PROCESS

To understand the thermal transfer technique used in an IR nondestructive testing system, the related heat transfer problem has

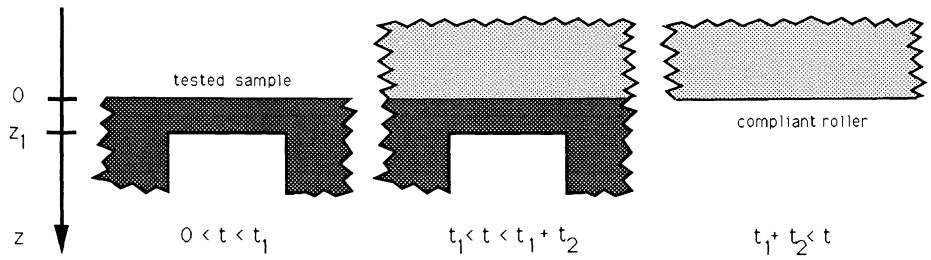

Fig. 4. The three phases of the thermal process.

to be analyzed; relevant physical parameters and optical configurations are thus pointed out. A realistic thermal flow model should be two or even three dimensional to take lateral diffusion into account, but when the lateral dimensions of the defect are large enough compared to the specimen thickness, a one-dimensional approach provides good insight on the thermal phenomena.[8,9]

The model corresponding to the configuration depicted in Fig. 1(a) will be further simplified in this way: (1) The sound parts of the tested material have a thickness that is sufficiently higher than the depth z_1 of the defect to be considered semi-infinite ($0<z<\infty$). (2) The defect has infinite resistance. In other words, the defective area has a thickness limited to z_1. (3) The compliant roller that takes the surface thermal print has a contact area large enough to produce a one-dimensional transfer between the two materials. Furthermore, the low conductivity of the roller makes it possible to ignore its finite diameter (roller material extending over $-\infty<z<0$).

The thermal process can be divided into three phases (see Fig. 4): (1) the surface temperature of the sample is heated by a Dirac energy pulse at time $t = 0$ and thereafter cools down (internal diffusion, absence of convection); (2) from time t_1 to t_1+t_2, the foam roller is brought in contact with the specimen and is more or less compressed; (3) at time t_1+t_2, the two materials are separated and the foam is correspondingly decompressed.

3.1. Temperature field during the first phase

The temperature increase distributions in finite and semi-infinite layers following a Dirac pulse at the surface $z=0$ are well known (Ref. 10, pp. 259 and 361). Within the tested material, one can write

$$T'_{\text{sound}_1} = \frac{Q}{\rho C\sqrt{\pi a t}} \exp\left(-\frac{z^2}{4at}\right) , \tag{1}$$

$$T'_{\text{defect}_1} = \frac{Q}{\rho C z_1}\left[1 + 2\sum_{n=1}^{\infty}\exp\left(-\frac{n^2\pi^2 at}{z_1^2}\right)\cos\left(\frac{n\pi z}{z_1}\right)\right] , \tag{2}$$

where ρ is the density (kg/m^3), C is the specific heat (J·kg^{-1}·K^{-1}), $a = k/\rho C$ is the thermal diffusivity (m^2/s), k is the thermal conductivity (W/mK), and Q is the absorbed energy per unit area (J/m^2).

The quantity $Q/\rho C z_1$ is equal to the final equilibrium temperature above the defect and will be used to normalize the temperatures to concentrate on the shape rather than the absolute levels of the temperature evolution curves (distances will be normalized by z_1 and times by z_1^2/a). The new notations will be $T = T'\rho C z_1/Q$ for the normalized temperature, z for the normalized distance, and $\text{Fo} = at/z_1^2$ for the Fourier number in the specimen; therefore,

$$T_{S_1} = T_{\text{sound}_1} = \frac{1}{\sqrt{\pi \text{Fo}}}\exp\left(-\frac{z^2}{4\text{Fo}}\right) , \tag{3}$$

$$T_{D_1} = T_{\text{defect}_1} = 1 + 2\sum_{n=1}^{\infty}\exp(-n^2\pi^2\text{Fo})\cos(n\pi z) . \tag{4}$$

The physical meaning of the Fourier number will be clearer when we consider that a Fourier number $\text{Fo}=1$ corresponds to a thermal propagation time $t=z_1^2/a$ of the thermal front to the depth z_1 of the defect.

3.2. Temperature field during the second phase

The temperature distribution in the sound region and in the foam above it may easily be found from the Green functions related to this configuration and presented in Ref. 10, p. 364.

The Green functions at $z\in[-\infty,\infty]$ for an instantaneous unit source at z' are expressed by

$$G_{S_2}(z\geq 0) = \frac{1}{2\sqrt{\pi \text{Fo}}}\left\{\exp\left[-\frac{(z'-z)^2}{4\text{Fo}}\right] + \frac{b-b_f}{b+b_f}\exp\left[-\frac{(z'+z)^2}{4\text{Fo}}\right]\right\} , \tag{5}$$

$$G_{S_2}(z\leq 0) = \frac{1}{\sqrt{\pi \text{Fo}}}\frac{b}{b+b_f}\exp\left[-\frac{\left(z'-z\sqrt{a/a_f}\right)^2}{4\text{Fo}}\right] , \tag{6}$$

where $b = \sqrt{k\rho C}$ is the sample effusivity (J·m^{-2}·K^{-1}·s$^{-1/2}$) and a_f and b_f are the foam diffusivity and effusivity. The physical meaning of thermal effusivity, whose square is usually referred to as thermal inertia,[7] can be understood by noticing that when a given heat power is absorbed at the surface of a material, its surface temperature rise is inversely proportional to its thermal effusivity.

By integrating these expressions, one obtains an interesting result for the case when two semi-infinite isothermal layers are brought in contact: the interface remains at a constant temperature that equates the mean of the initial temperatures weighted by the two material effusivities (this provides an explanation for the cooler sensation on our skin when it is brought in contact with a high effusivity cold metal piece as compared with an equally cold piece of wood of lower effusivity). In the present case, the foam layer is initially isothermal at the ambient temperature, but the sample layer has a temperature distribution as established at the end of the first phase ($\text{Fo}=\text{Fo}_1$).

The proper integration provides

$$T_{S_2}(z\geq 0) = \frac{1}{2\sqrt{\pi(\mathrm{Fo}+\mathrm{Fo}_1)}}\exp\left[-\frac{z^2}{4(\mathrm{Fo}+\mathrm{Fo}_1)}\right] \times \left(\mathrm{erfc}\left\{-z\left[\frac{\mathrm{Fo}_1}{4\mathrm{Fo}(\mathrm{Fo}+\mathrm{Fo}_1)}\right]^{1/2}\right\} + \alpha\,\mathrm{erfc}\left\{z\left[\frac{\mathrm{Fo}_1}{4\mathrm{Fo}(\mathrm{Fo}+\mathrm{Fo}_1)}\right]^{1/2}\right\}\right), \quad (7)$$

$$T_{S_2}(z\leq 0) = \frac{1}{(1+B)\sqrt{\pi(\mathrm{Fo}+\mathrm{Fo}_1)}}\exp\left[-\frac{z^2}{4A(\mathrm{Fo}+\mathrm{Fo}_1)}\right] \times \mathrm{erfc}\left\{-z\left[\frac{\mathrm{Fo}_1}{4A\mathrm{Fo}(\mathrm{Fo}+\mathrm{Fo}_1)}\right]^{1/2}\right\}, \quad (8)$$

where $A = a_f/a$, $B = b_f/b$, and $\alpha = (1-B)/(1+B)$.

The temperature calculation for the defective region and for the foam above it necessitates a prior evaluation of the Green functions associated with the present problem (instantaneous unit source at $z' \in [0, 1]$). By using the Laplace transform, the Green functions will be searched in the form

$$\overline{G_{D_2}}(z\geq 0) = \frac{1}{2\sqrt{p}}\{\exp(-\sqrt{p}|z'-z|) + \exp[-\sqrt{p}(2-z'-z)]\} + E\mathrm{ch}(\sqrt{p}z) + F\mathrm{sh}(\sqrt{p}z), \quad (9)$$

$$\overline{G_{D_2}}(z\leq 0) = H\exp(\sqrt{p}z), \quad (10)$$

where p is the Laplace variable. Constants E,F, and H will be provided by the boundary conditions at $z = 1$ (no heat flow) and at $z = 0$ (continuity of temperature and flow; thermal resistance at the contact interface is neglected). After some calculations and a Laplace inversion, one obtains

$$G_{D_2}(z\geq 0) = \frac{1}{2\sqrt{\pi\mathrm{Fo}}}\left(\exp\left[-\frac{(z'-z)^2}{4\mathrm{Fo}}\right] + \exp\left[-\frac{(2-z'-z)^2}{4\mathrm{Fo}}\right] + \sum_{n=0}^{\infty}\alpha^{n+1}\left\{\exp\left[-\frac{(2n+z'+z)^2}{4\mathrm{Fo}}\right] + \exp\left[-\frac{(2n+4-z'-z)^2}{4\mathrm{Fo}}\right] + \exp\left[-\frac{(2n+2+z'-z)^2}{4\mathrm{Fo}}\right] + \exp\left[-\frac{(2n+2-z'+z)^2}{4\mathrm{Fo}}\right]\right\}\right), \quad (11)$$

$$G_{D_2}(z\leq 0) = \frac{1}{(1+B)\sqrt{\pi\mathrm{Fo}}}\sum_{n=0}^{\infty}\alpha^n\left\{\exp\left[-\frac{(2n+z'-z/\sqrt{A})^2}{4\mathrm{Fo}}\right] + \exp\left[-\frac{(2n+2-z'-z/\sqrt{A})^2}{4\mathrm{Fo}}\right]\right\}. \quad (12)$$

Subsequent calculations will be simplified if the assumption is made that the first phase is sufficiently long compared to the thermal propagation time to the defect. If $\mathrm{Fo}_1 > 0.7$, the layer above the defect is nearly isothermal and one can therefore assume that $T_{\mathrm{defect}_1}(\mathrm{Fo}=\mathrm{Fo}_1) = 1$. This makes the integrations of the Green functions (11) and (12) easier to perform and provides

$$T_{D_2}(z\geq 0) = \frac{1}{2}\left\{\mathrm{erf}\left(\frac{z}{2\sqrt{\mathrm{Fo}}}\right) + \mathrm{erf}\left(\frac{2-z}{2\sqrt{\mathrm{Fo}}}\right) + \sum_{n=0}^{\infty}\alpha^{n+1}\left[\mathrm{erf}\left(\frac{2n+4-z}{2\sqrt{\mathrm{Fo}}}\right) - \mathrm{erf}\left(\frac{2n+z}{2\sqrt{\mathrm{Fo}}}\right) + \mathrm{erf}\left(\frac{2n+2+z}{2\sqrt{\mathrm{Fo}}}\right) - \mathrm{erf}\left(\frac{2n+2-z}{2\sqrt{\mathrm{Fo}}}\right)\right]\right\}, \quad (13)$$

$$T_{D_2}(z\leq 0) = \frac{1}{1+B}\sum_{n=0}^{\infty}\alpha^n\left[\mathrm{erf}\left(\frac{2n+2-z/\sqrt{A}}{2\sqrt{\mathrm{Fo}}}\right) - \mathrm{erf}\left(\frac{2n-z/\sqrt{A}}{2\sqrt{\mathrm{Fo}}}\right)\right]. \quad (14)$$

3.3. Temperature field during the third phase

When the sample and the foam are joined, the foam is compressed with a rate $\mu = \rho_f(\text{phase 2})/\rho_f(\text{phase 3})$; therefore, the effusivity of the foam may differ between phase 2 and phase 3. One notes that $B_f = b_f(\text{phase 3})/b_f(\text{phase 2})$ and $A' = a_f(\text{phase 3})/a$. For the last phase, only the thermal evolution in the foam is relevant since the infrared camera will record its surface temperature.

The combination of the distributions (8) and (14) at $\mathrm{Fo} = \mathrm{Fo}_2$ with the Green function in an isolated semi-infinite medium leads to the expressions

$$T_{S_3}(z\leq 0) = \frac{1}{2\pi(1+B)\sqrt{\mathrm{Fo}(\mathrm{Fo}_1+\mathrm{Fo}_2)}} \times \int_0^{\infty}\left\{\exp\left[-\frac{(z'+z/\sqrt{A'})^2}{4\mathrm{Fo}}\right] + \exp\left[-\frac{(z'-z/\sqrt{A'})^2}{4\mathrm{Fo}}\right]\right\} \times \exp\left[-\frac{B_f z'^2}{(\mathrm{Fo}_1+\mathrm{Fo}_2)}\right]\mathrm{erfc}\left\{z'\left[\frac{B_f\mathrm{Fo}_1}{4\mathrm{Fo}_2(\mathrm{Fo}_1+\mathrm{Fo}_2)}\right]^{1/2}\right\}dz', \quad (15)$$

$$T_{D_3}(z\leq 0) = \frac{1}{2(1+B)\sqrt{\pi\mathrm{Fo}}} \times \int_0^{\infty}\left\{\exp\left[-\frac{(z'+z/\sqrt{A'})^2}{4\mathrm{Fo}}\right] + \exp\left[-\frac{(z'-z/\sqrt{A'})^2}{4\mathrm{Fo}}\right]\right\} \times \sum_{n=0}^{\infty}\alpha^n\left[\mathrm{erf}\left(\frac{n+1+z'\sqrt{B_f}/2}{\sqrt{\mathrm{Fo}_2}}\right) - \mathrm{erf}\left(\frac{n+z'\sqrt{B_f}/2}{\sqrt{\mathrm{Fo}_2}}\right)\right]dz'. \quad (16)$$

One can notice that the foam *surface* temperature depends only on B, Fo_1, and Fo for the second phase and on B, B_f, Fo_1, Fo_2, and Fo for the third one. The diffusivity ratios A and A' are conditioning only the *internal* foam temperature.

3.4. Numerical simulations

For the experimental tests, which are presented in Sec. 5, the foam roller had been pressed to the tested samples so that the

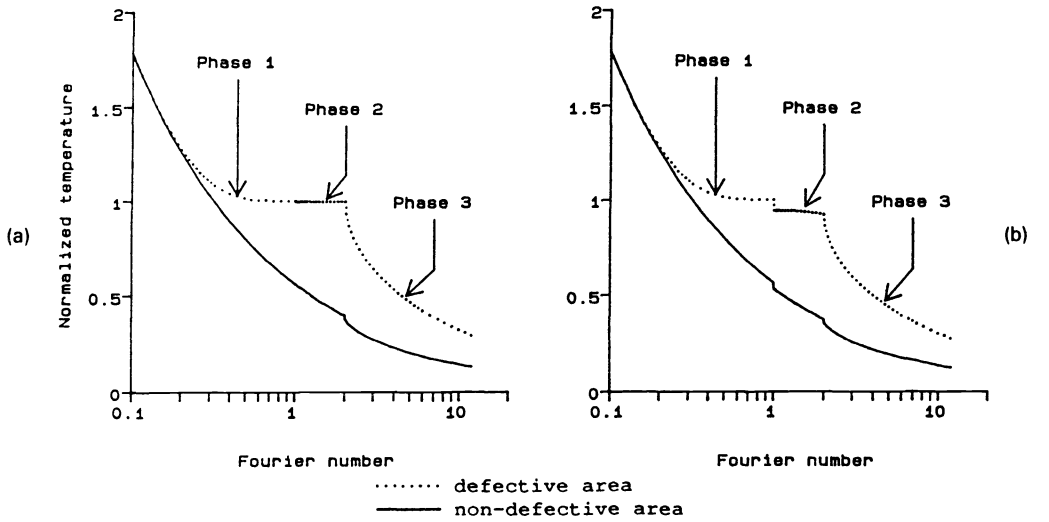

Fig. 5. Thermograms depicting the thermal transfer process for (a) high and (b) moderate effusivity materials.

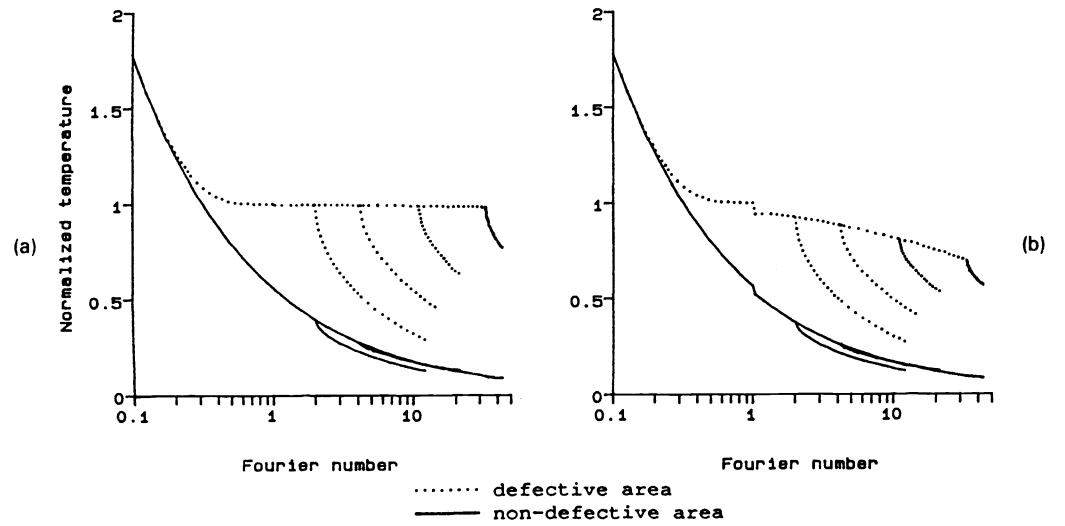

Fig. 6. Thermograms for the same materials as in Fig. 5, but for various second phase durations.

compression ratio reached about 2.5 within a layer more than 10 mm thick (e.g., 25 mm before compression and 10 mm after). Diffusivity and density measurements lead to the following results: ρ_f(phase 2) $\sim$ 12 kg/m^3, ρ_f(phase 3) $\sim$ 30 kg/m^3, C_f = 1650 J·kg^{-1}·K^{-1}, and k_f = 0.1 W/mK (which did not change substantially between the two phases).

The simulations reported in Fig. 5 are intended to describe the interface temperature evolution (z = 0) when high effusivity [5(a)] and moderate effusivity [5(b)] samples are tested. In the first case, in SI units, $b = 2.4\times10^4$ ($B = 3\times10^{-3}$), which corresponds to aluminum, whereas in the second case $b = 1.1\times10^3$ ($B = 6.3\times10^{-2}$) and can correspond to graphite-epoxy.

During the first phase (Fo_1 = 1), the normalized temperature tends toward 1 above the defect and toward 0 away from it. When the foam is pressed against the sample, one notices a step that becomes less pronounced as B gets smaller, and the temperature starts slowly to decay again above the defect. After the separation (Fo_2 = 1), the temperature abruptly decreases since no flow enters the foam anymore.

In Fig. 6 similar thermograms are reported but the second phase duration takes the values 1, 3.2, 10, 32, whereas Fo_1 = 1 and Fo_3 = 10. By comparing the third phase portion curves, one can easily see that the contrast between defective and sound regions will improve if the second phase is longer.

Those contrasts may be analyzed with respect to Fig. 7. The contrast, which could be observed directly on the surface of the sample if its emissivity were high, is represented by a dotted curve. Other contrasts corresponding to a noncompressed foam ($B = 1.9\times10^{-3}$ and B = 0.04, respectively) are also reported. A few remarks should be made as to the high Fourier number part of the curves: finite resistance and lateral size of a real defect lead to a decrease of the "direct imaging contrast" after a peak near Fo $\sim$ 1 to 10. The curves are therefore less and less representative of the ones describing a real defect as Fo exceeds 10. Nevertheless, one can conclude that thermal transfer imaging is less effective than direct imaging unless there is an emissivity problem, which hinders direct imaging. In that case, images should be picked up as soon as possible after the

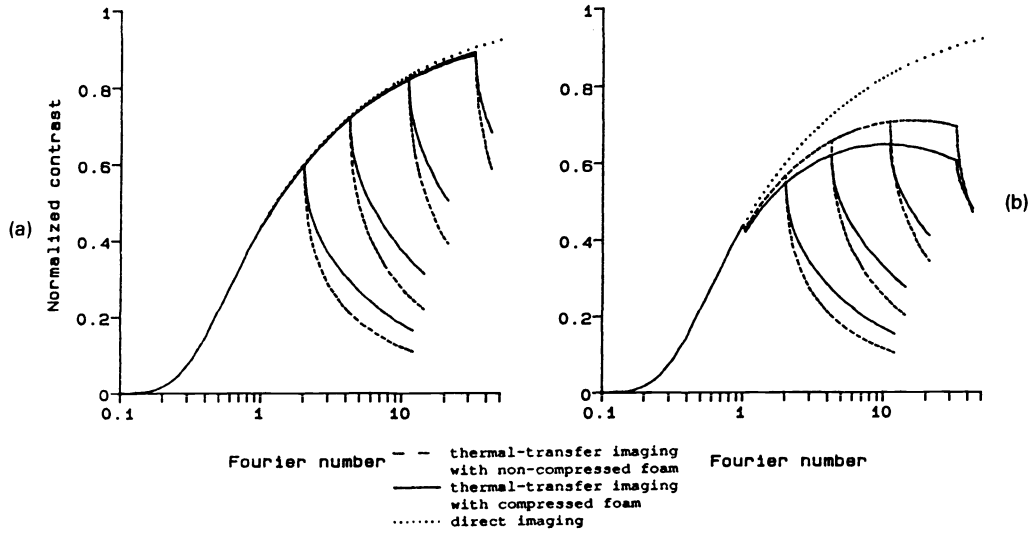

Fig. 7. Contrasts obtained with different imaging methods for the same materials as in Fig. 5.

separation. This makes the setup configuration of Fig. 2 more attractive than the configuration of Fig. 1. Noncompressed foam appears to give better results (B is lower), but this advantage vanishes shortly after the separation. Furthermore, at longer times, which are more convenient for image recordings, the compressed foam exhibits higher contrast and is thus more advantageous ($B_f < B$).

4. EXPERIMENTAL RESULTS

The thermal transfer imaging methods exposed in the previous sections were tested for the inspection of aluminum-to-foam laminates used in the transportation industry, in which potential defects are found in the epoxy layer that bonds the aluminum skin to the foam core. Furthermore, Plexiglas panels in which artificial defects were drilled on the back surface were tested. A 2500 W quartz IR lamp with a parabolic back reflector was used as a heat perturbation source. An AGEMA 782SW IR camera linked to our thermal inspection station[11] was used to pick up temperature images on the workpiece surface.

Figure 8(a) shows the compliant roller configuration in a reflective approach (heating and detection on the same side of the sample). Figure 8(b) shows some results obtained on the aluminum panel over a 2.5 cm diameter, 1 mm depth (aluminum skin) defect (artificially induced lack of epoxy at the foam interface) and on the Plexiglas plate (drilled hole 1 cm in diameter and 1.6 mm in depth). Three images are shown. On the left the black painted sample was tested in a reflective configuration with the IR camera pointed directly at the sample surface as the panel moves in the field of view after being heated by the lamp. The sample is mounted on a slide and moves at a speed of about 10 cm/s. Because of the high emissivity of the paint ($\varepsilon \sim 0.9$), the defect is clearly visible. The bright left bar is due to some edge effects during heating. A test done with the same but unpainted sample, directly imaged by the IR camera, did not reveal the defect because of the emissivity and reflectivity problems we mentioned previously. The right image shows the same sample but using the compliant roller configuration of Fig. 1 for transfer imaging [experimental apparatus of Fig. 8(a)]. This time, the IR camera was pointed at the roller surface. Although the thermal contrast is lower than in the previous case, where the camera picked up directly the thermal response of the defect, its appearance is still visible. In this latter case, we painted the sample black not for the transfer of the thermal contrasts to the roller but just for convenience, in order for the sample to be sufficiently stimulated by the heat source. Nevertheless, the transfer imaging process is demonstrated. The bright bar at the bottom is a direct view of the hotter black-painted sample, viewed by the camera positioned at an angle with respect to the roller-sample assembly. Figure 8(b) bottom shows an image from a test performed on the black-painted Plexiglas plate. The image transferred on the compliant roller shows the presence of the drilled hole. The plate was painted black to ensure surface heating on the transparent plate. An alternative to radiative heaters may be provided by contact heaters, air jets, or water sprays.[12] In this experiment, a foam roller 25 cm in diameter was pressed against the sample surface so that contact was established over an 11 cm length. In this trial it was unnecessary to cool the roller to erase the thermal printings on its surface because its circumference was shorter than the total sample length.

Figure 9(a) shows the experimental apparatus using the configuration of Fig. 2, where a closed-loop membrane (here made of rubber, 1.5 mm thick) serves to pick up the thermal contrasts. Figure 9(b) shows a reconstructed image[11] of a defect in the case of the aluminum laminate. The total setup size (heater, screen mask, and roller) over the workpiece surface was of the order of 10 cm, which is significantly less than the 30 cm in the case of the apparatus of Fig. 8. This space savings allowed, in the case of Fig. 9, detection of the defect even on the unpainted aluminum sample. This is because the heat flow propagation time in the aluminum surface layer is very small and the larger compliant roller configuration restricts the possibility of picking up the thermal contrast when it is already declining, thus preventing the detection unless stronger stimulation of the sample is performed. An air jet curtain was used to erase the thermal printings on the membrane.

Figure 10 presents results obtained on the aluminum panel with the configuration of Fig. 3. A high emissivity membrane is brought in contact with the high reflectivity sample surface to increase its emissivity. In this case, a thin (50 μm) black polyurethane film was brought in good thermal contact with the sample surface by water capillarity. The testing was done as explained for Fig. 8(b) left, resulting in the binary image shown in Fig. 10(a) after proper thresholding. No paint was applied on

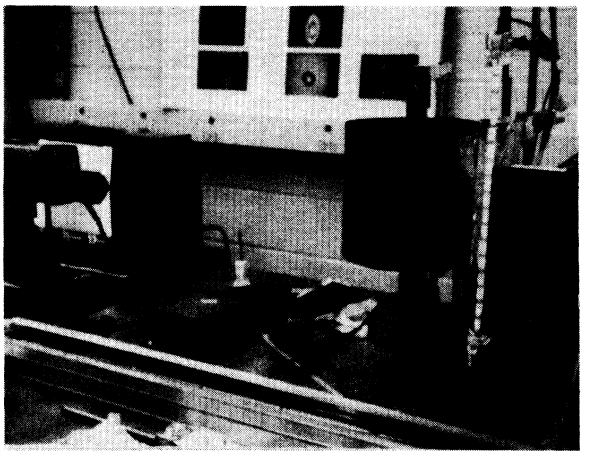

(a)

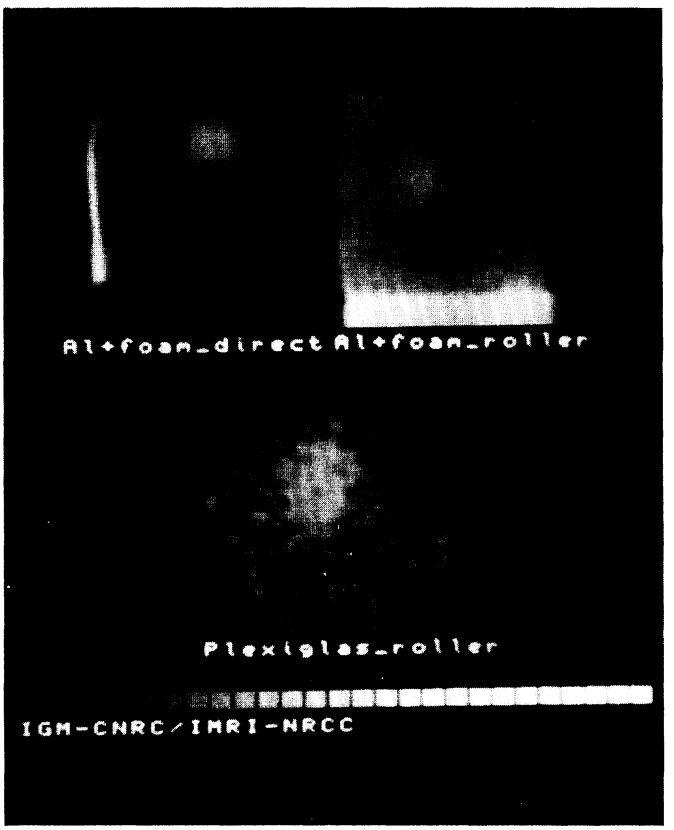

(b)

Fig. 8. (a) Experimental apparatus using the configuration of Fig. 1. The IR camera, compliant black roller, lamp heater, as well as the aluminum laminate mounted on a slide are visible. (b) Experimental results.

the surface. In Fig. 10(b) the same defect was detected but with the sample painted black and without using the polyurethane film. Comparison of Figs. 10(a) and 10(b) indicates a loss of thermal contrast. The time delay t of maximum defect visibility after thermal perturbation may be used to evaluate the depth z of the defect following the above-mentioned relation $z=(at)^{1/2}$. This is possible, in this case, because the whole temperature history of the sample is available, which was not the case for the previous configurations, where the thermal contrast was obtained at a given time only. For that reason, this configuration allows the detection of defects at various depths.

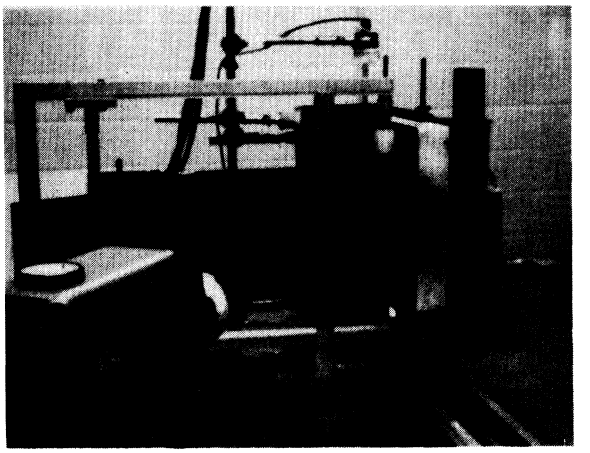

(a)

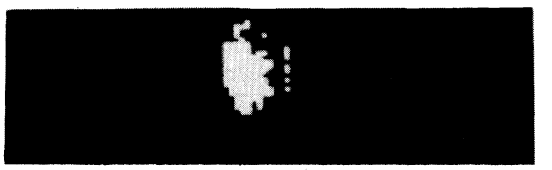

(b)

Fig. 9. (a) Experimental apparatus using the configuration of Fig. 2. The IR camera, compliant black roller and closed-loop membrane, lamp heater, as well as the aluminum laminate with white foam core mounted on a slide are visible. (b) Binary images of a defect.

(a)

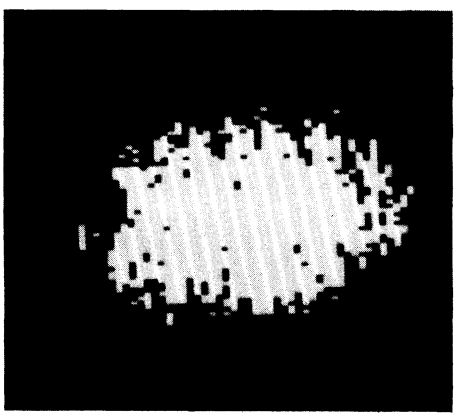

(b)

Fig. 10. (a) Binary image of a defect obtained with thermal-transfer imaging of Fig. 3. (b) Reference image of the same defect with black-painted sample and no membrane. Sample of Fig. 7.

5. CONCLUSION

Novel techniques for the nondestructive testing of highly reflective material by infrared thermography are proposed. Although yet at an early stage of development, these techniques of thermal transfer imaging are shown to have a strong potential because they address some of the main problems of thermography, namely, low emissivity and spurious reflections without being too complex to be deployed.

6. ACKNOWLEDGMENTS

B. Farahbakhsh of Alcan, Kingston Research Center, Ontario, is thanked for supplying the test samples.

7. REFERENCES

1. V. Vavilov, "Infrared nondestructive testing of bonded structures: aspects of theory and practice," Brit. J. NDT 22(4), 175–183 (1980).
2. W. Reynolds, "Quality control of composite materials by thermography," Metals and Materials 20(2), 100–102 (1985).
3. D. Balageas, A. Déom, R. Pujola, and D. Boscher, "Caractérisation et contrôle non destructif des composites carbone-époxy par méthode photothermique impulsionnelle," Qualité 25(139 bis), 43–47 (1986).
4. B. Rief, G. Busse, and P. Eyerer, "Nondestructive testing of carbon fiber reinforced plastics (CFRP) by thermal wave radiometry," in *Proc. 5th Int. Topical Meeting on Photoacoustic and Photothermal Phenomena,* P. Hess and J. Pelzl, eds., Springer-Verlag, Berlin, pp. 447–450 (1987).
5. P. Cielo, X. Maldague, A. Déom, and R. Lewak, "Thermographic NDE of industrial materials and structures," Materials Eval. 45(12), 452–480 (1987).
6. P. Cielo, J. C. Krapez, and M. Lamontagne, "Lumber moisture evaluation by a reflective cavity photothermal technique," Rev. Phys. Appliquée 23(9), 1565–1576 (1988).
7. K. O. Betty, Jr., and F. M. Richardson, "Transfer thermography," Mech. Eng. 43(10), 42–49 (1981).
8. J. Williams, S. Mansouri, and S. Lee, "One-dimensional analysis of thermal nondestructive detection of delamination and inclusion flaws," Brit. J. NDT 22(3), 113–118 (1980).
9. D. Balageas, J. C. Krapez, and P. Cielo, "Pulsed photothermal modeling of layered materials," J. Appl. Phys. 59(2), 348–357 (1986).
10. H. S. Carslaw and J. C. Jaeger, *Conduction of Heat in Solids,* Oxford Univ. Press (1959).
11. X. Maldague, J. C. Krapez, P. Cielo, and D. Poussart, "Inspection of materials and structures by infrared thermography: signal processing techniques for defect enhancement and characterization," Can. Soc. NDT J. 10(1), 28–35 (1989).
12. X. Maldague, P. Cielo, P. J. Ashley, and B. Farahbakhsh, "Thermographic NDT of aluminum laminates," Can. Soc. NDT J. 8(7), 44–50 (1987).

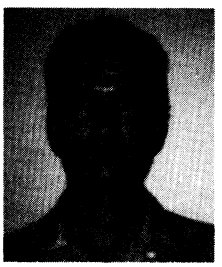

Xavier Maldague was with the National Research Council, Industrial Materials Research Institute, from 1984 to 1989, working on nondestructive evaluation techniques. Since 1989, Dr. Maldague has been an assistant professor in the Electrical Engineering Department of Université Laval, where he is involved in the field of infrared thermography. He also teaches courses in microprogramming, circuits theory, and industrial inspection. Dr. Maldague is a member of the IEEE and the Québec's professional engineers association (OIQ).

Jean-Claude Krapez received a diploma in engineering in 1984 from l'École Centrale de Paris, where he specialized in heat transfer. He was invited by the National Research Council Canada and joined the Optothermal Inspection Group at the Industrial Materials Research Institute in 1986, where he is working on the thermal characterization of industrial materials.

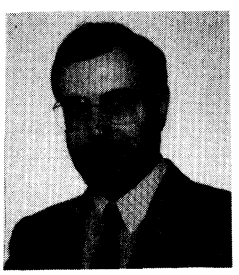

Paolo Cielo obtained his Ph.D. degree in optical physics from Laval University in Quebec in 1977. Prior to joining the Industrial Materials Research Institute, National Research Council Canada, in 1980, he was affiliated with Bell Northern Research, Ottawa, and with the Defence Research Establishment Atlantic in Dartmouth, Nova Scotia. Dr. Cielo is the author of more than 100 papers, 15 patents, and a textbook on optics-based techniques for industrial inspection (Academic Press, 1988).